



**POLITECNICO**  
MILANO 1863

**[RE.PUBLIC@POLIMI](#)**

Research Publications at Politecnico di Milano

## **Post-Print**

This is the accepted version of:

P. Múčka, L. Gagnon

*Influence of Tyre-Road Contact Model on Vehicle Vibration Response*

Vehicle System Dynamics, Vol. 53, N. 9, 2015, p. 1227-1246

doi:10.1080/00423114.2015.1041992

This is an Accepted Manuscript of an article published by Taylor & Francis in Vehicle System Dynamics, Vol. 53, N. 9, 2015, p. 1227-1246 on 21 may 2015, available online:

<http://www.tandfonline.com/10.1080/00423114.2015.1041992>.

Access to the published version may require subscription.

**When citing this work, cite the original published paper.**

Permanent link to this version

<http://hdl.handle.net/11311/1015463>

This is a post-print of an article:

MÚČKA, P., GAGNON, L. *Influence of tyre-road contact model on vehicle vibration response. Vehicle System Dynamics*, ISSN 0042-3114, Vol. 53, 2015, No. 9, pp. 1227-1246.

DOI: <http://dx.doi.org/10.1080/00423114.2015.1041992>

Web page: <http://www.tandfonline.com/doi/abs/10.1080/00423114.2015.1041992?journalCode=nvsd20#.V1rL2RkoMwA>

Publisher: Taylor & Francis

---

## Influence of tyre-road contact model on vehicle vibration response

Peter MÚČKA<sup>a,1</sup> and Louis GAGNON<sup>b</sup>

a) Institute of Materials and Machine Mechanics, Slovak Academy of Sciences,  
Račianska 75, SK-831 02 Bratislava 3, Slovak Republic

b) Department of Mechanical Engineering, Laval University, Avenue de la Médecine 1045,  
Québec City, Québec G1V 0A6, Canada

**Abstract:** The influence of the tyre-road contact model on the simulated vertical vibration response was analysed. Three contact models were compared: tyre-road point contact model, moving averaged profile and tyre-enveloping model. In total, 1600 real asphalt concrete and Portland cement concrete longitudinal road profiles were processed. The linear planar model of automobile with twelve degrees of freedom (DOF) was used. Five vibration responses as the measures of ride comfort, ride safety and dynamic load of cargo were investigated. The results were calculated as a function of vibration response, vehicle velocity, road quality and road surface type. The marked differences in the dynamic tyre forces and the negligible differences in the ride comfort quantities were observed among the tyre-road contact models. The seat acceleration response for three contact models and 331 DOF multibody model of the truck semi-trailer was compared with the measured response for a known profile of test section.

**Keywords:** road profile; tyre-road contact model; half car model; vibration; dynamic tyre force; ride comfort

### Introduction

The research on the excitation of the pneumatic tyres caused by uneven road surface was started in the 1960ies. The various enveloping models are currently used for prediction of the road-vehicle interaction system vibration: point contact models, roller contact models, empirical models, radial spring models, flexible ring models, footprint models, displaced area models, etc. [1]. The enveloping models were developed for describing the quasi-static tyre envelopment behaviour. The dynamic tyre models can generally be classified in the four categories: (a) rigid ring models, (b) multibody models, (c) finite element models, (d) modal models.

Eichberger and Schittenhelm [2] focused on the applications and limitations of the tyre models implemented in multibody codes. Lugner, Pacejka and Plöchl [3] described the tyre models which are able to reflect higher frequency ranges and account for local road surface structures. Rauh and Mössner-Beigel [4] provided an overview on the most challenging tasks for tyre simulation success in complete vehicle environments. A number of tyre models have been discussed and vehicle dynamic problems have been addressed in Pacejka [5]. In Li et al. [6], the various published tyre models used for vehicle dynamics and road loads analyses were compared in terms of their modelling approaches, applications and parameters identification process and methodologies. Some current tyre models intended for the vertical tyre dynamic was developed by Sandu and Umsrithong [7] (a multibody discrete tyre model) or Umsrithong and Sandu [8] (a semi-empirical stochastic transient tire model).

---

<sup>1</sup> Email: [ummsmuc@savba.sk](mailto:ummsmuc@savba.sk)

This study was intended to compare the three tyre-road contact models and their influence on the vertical vibration response. Many published research results used the vehicle models with the simple point contact assumption. Currently the tyre-road point contact is often used for computational simplicity and efficiency. Further, the simple filtration of the original profile with a moving average filter is currently used to avoid the necessity to simulate the tyre-road contact. The filtered road profile approximates the tyre envelopment of profile. Many complicated models intended for specific tasks of vehicle dynamics are currently used too. The tyre-enveloping model proposed by Schmeitz [1,9] was chosen as the representative of this category.

The presented study was intended to address the following:

- Model the vertical vibration response of a longitudinal planar vehicle model as a function of the tyre-road contact model and velocity;
- Estimate the difference among the three tyre-road contact models as a function of velocity, vibration response quantity, road roughness and road surface type;
- Study the influence of the three tyre-road contact models on the vibration response in the spatial domain as well as in the frequency domain;
- Compare the results for tyre-road contact models with an experiment based on parallel estimation of the road elevation and vibration response on vehicle.

### Road Profile Data

The road profile data for the left and right tracks from four Specific Pavement Studies (SPS) of the Long Term Pavement Performance (LTPP) program were analysed [10]. SPS-2 database contain doweled jointed plain concrete pavements, SPS-4 – rigid pavements, SPS-5 – rehabilitated asphalt concrete pavements and SPS-6 rehabilitated jointed Portland cement concrete (PCC) pavements. Two hundred profiles of the left track as well as the right track from each database were randomly chosen. In total, 1600 profiles were processed. The sampling interval of the original sections was  $\Delta l = 2.5$  cm with a typical section length about 150 m.

### Tyre-Road Contact Models

Three alternative tyre-road contact models (Figure 1) were considered:

1. A simple tyre-road point contact model – A raw profile serves as a direct input for a vehicle model (Figure 1a). This approach is the most extensively model used for computational simplicity. This model gives a fairly good approximation of the contact forces for profiles with prevalent long wavelengths [1,9].
2. Moving averaged road profile – The moving averaged profile simulates the tyre envelopment and is commonly used for the road profile data pre-processing purposes in profile analysis [11]. The moving average was found to reproduce test results for wavelengths larger than the base length of the moving average. The raw road profiles originally sampled with an interval  $\Delta l = 2.5$  cm were in this study pre-processed with a 30-cm moving average [Base length  $B = 30$  cm (Figure 1b)] and profiles were stored at interval of 15 cm. This approach is used for processing of measured profiles in Long Term Pavement Performance (LTPP) Program database [10].
3. Tyre-enveloping model – The rigid ring tyre model in combination with the tyre enveloping model [1,9] based on the tandem enveloping model with elliptical cams was applied in this study (Figure 1c). The unloaded tyre radius was considered to be  $R_0 = 0.31$  m. The effective road plane obtained for constant ellipse parameters was calculated and was used as an input into the vehicle model. The mean values of dimensionless tandem base length end ellipse parameters identified for five tyre models [1,9] were considered.

### Longitudinal Planar Model of an Automobile

The planar model of an automobile [12] used has 12 DOF (Figure 2). The human body model according to the ISO 5982: 2001 [13] was used. The natural frequencies of the 12-DOF model were:  $f_{\phi 2} = 1.12$  Hz (vehicle body pitching),  $f_{x2} = 1.08$  Hz (vehicle body bouncing),  $f_{x5d} = 3.40$  Hz (mass  $m_{5d}$  bouncing),  $f_{x5p} = 3.55$  Hz (mass  $m_{5p}$  bouncing),  $f_{x4d} = f_{x4p} = 5.42$  Hz (masses  $m_{4d}$  and  $m_{4p}$  bouncing),  $f_{x1f} = 10.93$  Hz

(front axle bouncing),  $f_{x1r} = 12.88$  Hz (rear axle bouncing),  $f_{x6d} = f_{x6p} = 24.29$  Hz (masses  $m_{6d}$  and  $m_{6p}$  bouncing),  $f_{x3d} = f_{x3p} = 35.14$  Hz (masses  $m_{3d}$  and  $m_{3p}$  bouncing).

The vehicle model parameters were as follows [12]: front and rear wheel,  $m_{1f} = 70$  kg;  $m_{1r} = 50$  kg,  $k_{1f} = k_{1r} = 3e6$  N/m; vehicle body mass,  $m_2 = 1000$  kg, vehicle body moment of inertia  $I_2 = 1430$  kg m<sup>2</sup>, vehicle body suspension,  $k_{2f} = 3e4$  N/m,  $b_{2f} = 2842$  Ns/m,  $k_{2r} = 2.7e4$  N/m,  $b_{2r} = 2462$  N/m, seat suspension,  $k_{3d} = k_{3p} = 50210$  N/m,  $b_{3d} = b_{3p} = 276$  Ns/m.

The parameters of the human body model were as follows [13]:  $m_{3d} = m_{3p} = 2$  kg,  $m_{4d} = m_{4p} = 45$  kg,  $k_{4d} = k_{4p} = 36200$  N/m,  $b_{4d} = b_{4p} = 1390$  Ns/m,  $m_{5d} = m_{5p} = 6$  kg,  $k_{5d} = k_{5p} = 9999$  N/m,  $b_{5d} = b_{5p} = 387$  Ns/m,  $m_{6d} = m_{6p} = 2$  kg,  $k_{6d} = k_{6p} = 34400$  N/m,  $b_{6d} = b_{6p} = 234$  Ns/m. The masses 3–6 present the sitting human body model defined in ISO 5982: 2001. This model is an approximation of human body response based on the human body apparent mass as well as on the vibration transmissibility to the head. There is no direct correlation between the human body model masses 3–6 and various body segments.

Dimensions of the vehicle model were:  $d_f = 1.1$  m,  $d_r = 1.3$  m,  $d_d = 0.42$  m, and  $d_p = 1$  m. The static tyre force is 6 kN for the front axle and 5.2 kN for the rear axle. The model resonance frequencies cover a typical range of resonances for unsprung and sprung masses of a real automobile. Model was used as the sample representative of the vehicle fleet.

## Simulation Results

The vehicle model was built and all the computations were provided in Matlab/Simulink environment. Fixed sampling step  $\Delta t = 1e-3$  s was used. The vehicle model response was obtained numerically in the time-domain with fourth order Runge-Kutta method.

The root mean square (RMS) values of five vertical vibration responses were calculated:

- Driver's seat (mass  $m_{3d}$ ) frequency-weighted vertical acceleration,  $a_{wds}$ ;
- Passenger's seat (mass  $m_{3p}$ ) frequency-weighted vertical acceleration,  $a_{wps}$ ;
- Front axle dynamic tyre force RMS value  $F_{dF}$ ;
- Rear axle dynamic tyre force RMS value  $F_{dR}$ ;
- Car body centre of gravity (CG) vertical acceleration,  $a_{cb}$ .

Frequency-weighted accelerations are measures of ride comfort, the dynamic tyre forces are measures of the ride safety and dynamic load of road and car body acceleration is a measure of the dynamic effect on the cargo.

For the frequency weighting of simulated acceleration response, the filter  $W_k$  intended for the vertical acceleration on the seat surface defined in the ISO 2631-1: 1997 [14] was used.

The variable  $\Delta$  presents the percentage difference between RMS values of vibration response for the  $i$ -th and  $j$ -th tyre-road contact model:

$$\Delta (\%) = 100 \times \frac{\text{RMS}\{\text{vibr.response}\}_i - \text{RMS}\{\text{vibr.response}\}_j}{\text{RMS}\{\text{vibr.response}\}_j} \quad (1)$$

A right track of the doweled jointed plain concrete road section #040214K1 [10] of poor surface condition measured in December 2004 was used for analysis (Figure 3). Functional class of this road is "Rural Principal Arterial – Interstate". The section was constructed in 1993. Figure 4 presents calculated vibration response presents for all three tyre-road contact alternatives. Two vibration responses for three velocities  $v = 60, 90$  and  $120$  km/h are shown. The acceleration responses (left column of Figure 4) are similar because the response function of frequency-weighted acceleration  $a_{wds}$  suppressed the short-wavelength contents and this response is the most sensitive to the frequency range 4–8 Hz, i.e. to the wavelengths  $L = 2.1$ – $4.2$  m for  $v = 60$  km/h,  $L = 3.1$ – $6.3$  m for  $v = 90$  km/h and  $L = 4.2$ – $8.3$  m for  $v = 120$  km/h. The differences between profiles were observed at short wavelengths for  $F_{dR}$  response (right column of Figure 4).

Table 1 presents the percentage differences in vibration response RMS values (Eq. (1)) for the test section #040214K1. The vibration response RMS values were the lowest for the tyre-enveloping model and the highest for the tyre-road point contact model. The moving averaged profile caused slightly higher response than the tyre-enveloping model. The differences are apparent at all three velocities.

The difference between response RMS values decreased with velocity increase. The similar tendencies were observed for all three models and ride comfort quantities,  $a_{\text{wds}}$  and  $a_{\text{wps}}$ . The mean difference among models was below 2 %. The highest differences were calculated for the dynamic tyre forces. About 22–27 % decrease of the tyre force RMS value was observed for the moving averaged profile in comparison to the tyre-road point contact and  $v = 60$  km/h. The tyre-enveloping model caused lower response by 5–15 % in relation to the tyre-road point contact model. The tyre-enveloping model caused higher response by 3–15 % as those calculated for the moving averaged profile. The moving averaged profile model slightly underestimates the vibration response in comparison with the tyre-enveloping model. The differences in car body acceleration were below 6 %.

Figures 5 and 6 present the influence of the road elevation spectrum, velocity, and transfer function on the vibration response spectrum for acceleration  $a_{\text{wds}}$  (Figure 5) and dynamic tyre force  $F_{\text{dR}}$  (Figure 6). The 12-DOF vehicle model (Figure 2) was kinematically excited by the right track of the measured profile #040214K1.

Figure 5 shows the influence of the tyre-road contact models on the frequency-weighted driver's seat acceleration spectrum,  $G_{\text{awds}}$ . The first row shows how the road spectrum is shifted to the right, i.e., to the higher temporal frequencies corresponding to the same wavelengths ( $f = v/L$ ). The long wavelengths contribute the most to the road elevation power. The road spectrum decreases approximately with power two of frequency. The magnitude of the transfer function estimate,  $|H_{\text{awds}}(f)|$ , between road elevation and acceleration,  $a_{\text{wds}}$  (second row of Figure 5), is dependent on the velocity because it is influenced by the excitation time delay between a particular axle and a measuring point, i.e., driver's seat. The resonance frequencies of human body–seat system (2–5 Hz) and axle wheel-hop bounce ( $\sim 10$  Hz) are the most amplified by vehicle model. The filter  $W_k$  (ISO 2631-1) intended for the vertical acceleration on the seat surface markedly amplified a frequency band 4–8 Hz. The theory of the transfer function of the half-car model was comprehensively addressed in Mitschke and Wallentowitz [15]. The third row of Figure 5 shows differences in acceleration spectrum,  $G_{\text{awds}}$ . The spectrum corresponds to multiplication of the road elevation power spectral density (PSD) by a square of the transfer function  $|H_{\text{awds}}(f)|^2$ . The RMS value of the acceleration response corresponds to the square root of the area under the spectrum,  $G_{\text{awds}}$ . A contribution of the low frequencies about 1 Hz increased with velocity. The amplification of this frequency band increased with velocity as is shown on transfer function estimate in the second row of Figure 5. The differences in the spectrum were negligible among the tyre-road contact models.

Figure 6 shows the spectrum of the rear-axle dynamic tyre force,  $G_{\text{FDR}}$ , for a 12-DOF automobile model. The transfer function between road elevation and tyre force markedly amplifies the frequency band at wheel-hop resonance ( $\sim 10$  Hz). The differences among the tyre-road contact models were apparent in the frequency band above 10 Hz. This frequency band corresponds to the short wavelengths  $L < v/f$ , i.e.  $L < 1.7$  m (60 km/h),  $L < 2.5$  m (90 km/h) and  $L < 3.3$  m (120 km/h). A contribution of low frequencies of about 1 Hz to the total signal power increased with velocity. The largest differences in the response spectrum were observed for  $v = 60$  km/h and differences decreased with velocity.

## The Influence of Road Quality

The road roughness quality was quantified by International Roughness Index (IRI), which is worldwide used indicator in Pavement Management System [11]. The IRI is essentially a computer-based virtual-response-type system based on the response of a quarter-car vehicle model as it traverses a tested pavement section at a constant speed of 80 km/h [16].

The measured data based on parallel estimation of the road elevation and vibration response on vehicle are rare. The relations between the IRI and ride comfort quantities based on the in-situ measurement were provided by Ahlin et al. [17] and Hassan and McManus [18] for truck semi-trailer, by Ihs et al. [19] for passenger car, by Fichera et al. [20] for bus, by Zhang et al. [21] for a multi-function test vehicle, by Lee et al. [22] for van or by Cantisani and Loprencipe [23] for a passenger car model.

The relations between the IRI and dynamic tyre forces were provided by Papagiannakis and Woodroffe [24] or by Kulakowski et al. [25] for heavy trucks, by Magnusson, Dahlstedt and Sjögren [26] for laser road deflection tester, by Jacob and Dolcemasclo [27] for a single axle instrumented trailer, by Elischer et al. [28] and Chen et al. [29] for three-axle semi-trailers. A short overview of the measured and simulated relations between IRI and vehicle vertical vibration response was provided in

Můčka [30]. The linear relation between IRI and vehicle vibration response RMS values was often observed [17–30].

Figure 7 presents the percentage difference  $\Delta$  (Eq. (1)) among three contact alternatives for 1600 randomly chosen profiles of SPS-2, SPS-4, SPS-5 and SPS-6 databases as a function of the road unevenness indicator IRI and velocity. The difference  $\Delta$  slightly decreased with increase of the road roughness for  $F_{dR}$  response. The lower dependence on the road roughness was observed for both accelerations  $a_{wds}$  and  $a_{cb}$ . The dependence on the road roughness was more pronounced at velocity  $v = 60$  km/h. The difference slightly increased with the increase of road roughness for car body acceleration  $a_{cb}$ .

Table 2 shows the mean difference among the contact models for 1600 road profiles. A difference among response RMS values decreased with velocity increase. The similar tendencies were observed for all three contact models and the ride comfort measures,  $a_{wds}$  and  $a_{wps}$ . The mean difference was below 2 %. The highest differences were calculated for the dynamic tyre forces. About 20 % decrease in the tyre force response was observed for the moving averaged profile in comparison to the tyre-road point contact and  $v = 60$  km/h. The tyre-enveloping model caused lower response by 5–10 % in comparison with the tyre-road point contact model. The tyre-enveloping model caused higher response by 3–15 % as those calculated for the moving averaged profile.

Road quality indicator IRI is limited to reflect the short-wavelength contents of the profile elevation [31,32]. The road vertical elevation spectrum parameters were used as an alternative road unevenness indicator to the IRI. The simplest model of the road elevation PSD  $G_H(\Omega)$  is often applied in the form [33,34]

$$G_H(\Omega) = C\Omega^{-w} \quad (2)$$

where  $\Omega$  (rad/m) is the angular spatial frequency,  $C$  ( $\text{rad}^{w-1} \text{m}^{3-w}$ ) =  $G_H(1)$  is the unevenness index, and  $w$  is the waviness. The example of the measured road elevation and road elevation PSD is presented in Figure 8. Eq. (2) represents a line on a log-log chart with  $C$  as the vertical ordinate at the reference angular frequency  $\Omega_0 = 1$  rad/m and  $w$  as the slope of the line. Parameters  $C$  and  $w$  are independent. While  $C$  is proportional to the unevenness variance,  $w$  expresses the wavelength distribution between particular spatial frequency bands. The interpretation of the waviness value is the following: for  $w = 2$ , the individual wavelengths in the road elevation PSD are present in similar proportions; for  $w > 2$ , the long wavelength contents is prevalent; for  $w < 2$ , the short wavelength contents is prevalent. The waviness of in-service roads moves in a broad interval from 1.5 to 3.5 [33,35,36]. The ISO 8608 defines the fitting interval of the raw PSD by a straight line in the angular spatial frequency range of 0.069–17.77 rad/m. The influence of the road waviness on the vibration response for the tyre-road point contact model was analysed in [34,37–39].

Figure 9 shows that the difference among the contact models slightly decreased with increase of the unevenness index  $C$  in case of the tyre force response and is practically independent for both acceleration responses. The difference was strongly dependent on the waviness. It seems logical because the lower waviness corresponds to the profiles with the prevalent short-wavelength contents which results to the more pronounced differences among three contact models.

### The Influence of Road Surface Type

Figure 10 shows the influence of the road surface type on the differences in dynamic tyre force  $F_{dR}$  between the tyre-enveloping model and the tyre-road point contact model for three velocities. It is apparent how the difference among the contact models decreased with increase of road roughness in case of jointed plain concrete pavements (SPS-2) and rigid pavements (SPS-4) in the range of IRI = 1–2 mm/m. This tendency was less pronounced for asphalt concrete pavements (SPS-5) and rehabilitated jointed PCC pavements (SPS-6). The chosen samples from these two databases contain more profiles of lower quality with IRI > 2 mm/m. The rapid change in differences was calculated for profiles with IRI < 1.5 mm/m. For road sections with IRI > 2 mm the changes in difference were less pronounced. Figure 10 indicates that the differences among the contact models are lower for higher velocities.

Table 3 shows the mean difference in response as a function of the road surface type for  $v = 90$  km/h. In the second column of Table 3 the mean value and standard deviation of the IRI were issued. Four

hundred profiles from each database were processed. The mean difference in a response only slightly varied with the surface type.

## Experimental Results

A short experimental study was provided on vibration response data that were recorded on a real semi-trailer truck on a test section with the known elevation [40]. The experimental results were compared with a 331 DOF multibody semi-trailer truck model with three alternative tyre road contact models: tyre-road point contact, moving averaged road profile and the more complex tyre model – a rigid ring tyre model developed by Gagnon et al. [41,42]. The road section “Essais AM” (Run 8) was used of the length of 714.03 m sampled at the interval 0.5 cm (Figure 11a). The road spectrum,  $G_H(\Omega)$ , for this test section is shown in Figure 11b. The experiment was provided on three-axle tractor with a three-axle semi-trailer with a total weight of 43 t. The average velocity of the semi-trailer truck on the section was 67 km/h. The measured vertical acceleration response on driver’s seat surface is shown in Figure 11c. The corresponding spectrum for acceleration  $a_s$  and frequency-weighted acceleration  $a_{ws}$  is shown in Figure 11d.

The real semi-trailer truck was implemented as a multibody model [40]. The model has 331 DOF including the tyres. Apart from the wheels, the model has 13 rigid bodies each having 6 DOF: one for each axle; one for the chassis frame and the components which are rigidly attached to it, such as the batteries and gas tanks; one for the engine; one for the cabin; one for the driver and one for the passenger; one for the radiator; and one for the semi-trailer frame.

An implicit ring tyre model was implemented into the free software MBDyn. The model is largely based on the Short Wavelength Intermediate Frequency Tire (SWIFT) model developed by Pacejka [5] and the road filtering used by Schmeitz [1,9]. The rigid ring tyre model takes the three-dimensional forces and moments coming from the wheel of the truck model as one input. The model takes 45 tyre parameters and 20 algorithm parameters and is integrated implicitly except for the road profile.

Figure 12 shows a possible influence of three tyre-road contact models on the measured acceleration. The effective road plane for the tyre-enveloping model was calculated for the parameters of the truck wheel: unloaded tyre radius,  $R_0 = 0.52$  m, vertical load of tyre,  $F_{nom} = 3.43e4$  N and the tyre radial stiffness,  $k = 1e6$  N/m.

Figure 12a shows the road elevation spectrum,  $G_H(f)$ , of the left track for the real road section “Essais AM” and velocity  $v = 67$  km/h as a function of the tyre-road contact model. The spectrum decreased approximately with square of frequency. The higher differences were observed for frequencies above 20 Hz. Figure 12b shows the transfer function estimate,  $|H_{aws}(f)|$ , between road elevation,  $h_L$ , and measured frequency-weighted seat vertical acceleration,  $a_{ws}$ . Figure 12c shows the spectrum of frequency-weighted measured seat acceleration,  $G_{aws}$ . The contribution of the frequencies above 20 Hz is negligible. The small differences among the frequency-weighted RMS accelerations can be expected for these three analyzed tyre-road contact models. The tyre-enveloping model in Figure 12a shows the larger differences in comparison with the tyre-road point contact model and moving averaged profile as was presented in Figs. 5 and 6 for a passenger car. The differences are caused by the different unloaded tyre radius,  $R_0 = 0.52$  m (Figure 12, truck) and  $R_0 = 0.31$  m (Figures 5 and 6, passenger car).

Table 4 presents the measured and simulated seat RMS accelerations for three tyre-road contact models in 100-m long segments of “Essais AM” test section for  $v = 67$  km/h. The multibody semi-trailer truck model with 331 DOF was used [40]. The road roughness indicators IRI and road elevation spectrum parameters  $C$  and  $w$  are also shown in Table 4. The indicators for parallel tracks were calculated as follows:  $IRI_{LR} = (IRI_L + IRI_R)/2$ ,  $C_{LR} = \sqrt{C_L C_S}$ ,  $w_{LR} = (w_L + w_R)/2$ . Figure 13 shows a time response of frequency-weighted acceleration  $a_{ws}$  for measured and simulated response for three tyre-road contact models.

By analysis of the results, the following conclusions can be reached:

- The measured frequency-weighted RMS accelerations are higher than the simulated ones. According to Gagnon [40] the 331 DOF multibody model of the truck semi-trailer was able to fit the response at lower frequencies. The RMS value for filtered signal of measured acceleration in the frequency band 0.2–10 Hz was added in Table 4.

- The velocity of the semi-trailer truck measured response was not a constant. The used velocity  $v = 67$  km/h is an approximation based on the time of response measurement and length of section. The variable velocity could cause the differences in Table 4.
- The complex rigid ring tyre model did not show the better results (i.e., closer to the measured response) than the tyre-road point contact model and moving averaged profile (Table 4) in all particular 100-m parts of analysed section. It is difficult to compare the analysed tire models predictions with real acceleration response on a vehicle because not only tyre model but the vehicle model affects the vibration response too. The rigid ring tyre model used the tyre enveloping according to the Schmeitz's approach [9]. The unloaded tyre radius is higher for truck than for a passenger car ( $R_0 \sim 0.52$  m vs.  $R_0 = 0.31$  m).
- The results for TRPC and MA contact models are similar and show negligible differences to those obtained by simulation of passenger car in Figs. 5 and 6 and Tables 1 and 2.

## Conclusions

A limited number of studies have addressed the important question of the difference in vertical vibration response as a function of the tyre-road contact models based on the broad database of the real road sections. This study was based on the processing of 1600 road sections from the LTPP database and three tyre-road contact alternatives. The main results of this study were:

1. The differences between the tyre-road contact models were function of velocity, frequency contents of the road profile vertical displacements and frequency contents of the vibration response. The differences between the contact models were apparent at higher frequencies above 10 Hz. The vibration quantities with marked frequency contents contribution at higher frequencies showed the marked differences in vibration response.
2. The tyre-road contact models were found to have only a marginal influence on the ride comfort measures. The observed differences were below 3 % for the frequency-weighted acceleration on the driver's and passenger's seats and below 6 % for the car load acceleration.
3. The tyre-road contact models were found to have marked impact on the dynamic tyre forces. The differences increased with velocity decrease. The highest tyre forces were calculated for the tyre-road point contact model. The tyre-enveloping model showed higher dynamic tyre forces RMS values (by 5–10 % for  $v = 90$  km/h) than the moving averaged profile.
4. The road roughness influenced the differences among the tyre-road contact models. The differences decreased with increase of the road roughness for the ride safety measures and were practically constant for the ride comfort measures. The differences slightly increased with increase of the road roughness for the car load acceleration. The poor quality profiles with  $IRI > 2$  mm/m have showed lower percentage differences in vibration response as the better road sections.
5. The road surface type found to have negligible effect on the differences among the contact models.
6. The dependence of the difference among the contact models on the road elevation spectrum parameters showed that the difference only slightly decreased with unevenness index increase and strongly decreased with waviness increase.
7. The frequency contents of the measured acceleration response and the measured road elevation indicates a possible small influence of the tyre-road contact models on the ride comfort quantities.

## Acknowledgement

This work was supported by the VEGA Grant Agency of the Slovak Academy of Sciences under Grant No. 2/0058/13. The help of the LTPP InfoPave Support Team is highly appreciated.

## REFERENCES

- [1] Schmeitz A.J.C. A semi-empirical three-dimensional model of the pneumatic tyre rolling over arbitrarily uneven road surfaces. [PhD Thesis]. Technische Universiteit Delft, Delft, Netherlands, 2004.
- [2] Eichberger A., Schittenhelm M. Implementations, applications and limits of tyre models in multibody simulation. *Veh. Syst. Dyn.* 2005; 43(S1): 18–29.
- [3] Lugner P., Pacejka H., Plöchl M. Recent advances in tyre models and testing procedures. *Veh. Syst. Dyn.* 2005; 43(6–7): 413–426.
- [4] Rauh J., Mössner-Beigel M. Tyre simulation challenges. *Veh. Syst. Dyn.* 2008; 46(S1): 49–62.
- [5] Pacejka H. *Tire and vehicle dynamics*. 3<sup>rd</sup> Ed., Oxford, UK : Butterworth-Heinemann, 2012, 672 p.
- [6] Li B., Yang X., Yang J. Tire model application and parameter identification – a literature review. *SAE Int. J. Passeng. Cars – Mech. Syst.* 2014; 7(1): 231–243.
- [7] Sandu, C., Umsrithong, A. Discrete mass tyre model for ride investigation over uneven rigid terrain. *Int. J. Veh. Des.* 2014; 66(1): 87–106.
- [8] Umsrithong A., Sandu, C. Stochastic transient tyre model for vehicle dynamic simulations on rough terrain. *Int. J. Veh. Syst. Model. Test.* 2012; 7(4): 351–371.
- [9] Schmeitz A.J.C., Jansen S.T.H., Pacejka H.B., Davis J.C., Kota N.M., Liang C.G., Lodewijks G. Application of a semi-empirical dynamic tyre model for rolling over arbitrary road profiles. *Int. J. Veh. Des.* 2004; 36(2–3): 194–215.
- [10] LTPP InfoPave [online]. (2014). Federal Highway Administration, US Department of Transportation, Available from: [www.infopave.com](http://www.infopave.com) [Accessed 20 February 2014].
- [11] Sayers M.W., Karamihas S.M. *The little book of profiling*. Ann Arbor, MI : University of Michigan; 1998.
- [12] Stein G.J., Múčka P. Theoretical investigation of a linear planar model of a personal car with seated people. *Proc. Inst. Mech. Eng. Part D. – J. Automobile Eng.* 2003; 217(4): 257–268.
- [13] ISO 5982, Mechanical vibration and shock—range of idealized values to characterize seated-body biodynamic response under vertical vibration, International Organization for Standardization, Geneva, 2001.
- [14] ISO 2631-1, Mechanical vibration and shock – evaluation of human response to wholebody vibration. Part I: general requirements, International Standardization Organization, Geneva, 1997.
- [15] Mitschke M., Wallentowitz H. *Dynamik der Kraftfahrzeuge*. 4<sup>th</sup> Ed., Berlin: Springer Verlag; 2004.
- [16] Sayers M.W. On the calculation of IRI from longitudinal road profile. *Transportation Research Record 1501*, Transport Research Board, Washington, DC, 1995.
- [17] Ahlin K., Granlund J., Lundström R. Whole-body vibration when riding on rough roads – A shocking study. Report 2000:31E, Swedish Road Administration, Borlange, Sweden, 2000, 81 p.
- [18] Hassan R.A., McManus K. Assessment of interaction between road roughness and heavy vehicles. *Transp. Res, Record 1819*, Washington, DC: Transportation Research Board, 2003; 236–243.
- [19] Ihs A., Grudemo S., Wiklund M. The influence of road surface condition on driving comfort. VTI Report No. 957, Swedish National Road and Transport Research Institute, Linköping, Sweden, 2004, 131 p. (in Swedish).
- [20] Fichera G., Scionti M., Garescì F. Experimental correlation between the road roughness and the comfort perceived in bus cabins. *SAE Technical Paper 2007-01-0352*, 2007.
- [21] Zhang J., Du Y., Su R. Investigating the relationship between pavement roughness and heart-rate variability by road driving test. *Proc. of the 3<sup>rd</sup> International Conference on Road Safety and Simulation*, 14–16 September 2011, Indianapolis, USA, Purdue University & Transport Research Board, 2011.
- [22] Lee D.-H., Kim J.-W., Mun S.-H., Jeong W.-S. Study about the Evaluation of Driving Stability Using 3-axis Accelerometer Test. *J. of the Korean Society of Road Engineers* 2012; 14(3): 141–149.
- [23] Cantisani G., Loprencipe G. Road roughness and whole body vibration: evaluation tools and comfort limits. *J. Transp. Eng.* 2010; 136(9): 818–826.

- [24] Papagiannakis A.T., Woodrooffe J.H.F. Suitability of alternative pavement roughness statistics to describe dynamic axle loads of heavy vehicles. Proc. of the 2<sup>nd</sup> Int. Symposium on Heavy Vehicle Weights and Dimensions, Transportation Association of Canada, Ottawa, Canada, 1989.
- [25] Kulakowski B.T., Streit D.A., Wollyung R.J., Kenis W.J. A study of dynamic wheel loads conducted using a four-post road simulator. Proc. of 4<sup>th</sup> International Symposium on Heavy Vehicle Weights and Dimensions, June 25-29, 1995, Ann Arbor, MI, Transportation Research Institute, University of Michigan, 1995, 301–307.
- [26] Magnusson G., Dahlstedt S., Sjögren, L. Measurements of the road surface longitudinal unevenness—methods and necessary accuracy. [in Swedish]. VTI Report 475, Swedish National Road and Transport Institute, Sweden, 2002, 94 p.
- [27] Jacob B., Dolcemascolo V. Dynamic interaction between instrumented vehicles and pavements. Proc. of 5th International Symposium on Heavy Vehicle Weights and Dimensions, Maroochydhore, Queensland, Australia, ARRB Group Limited, Victoria, 1998, 142–160.
- [28] Elischer M., Trevorrow N., Callaway L., Blanksby C. Measuring and analysis of dynamic wheel loads. Rep. AP-R406-12, Austroads, Sydney, New South Wales, 2012.
- [29] Chen Y., He J., King M., Chen W., Zhang W. Effect of driving conditions and suspension parameters on dynamic load-sharing of longitudinal-connected air suspensions. Science China Technological Sciences 2013; 56(3): 666–676.
- [30] Můčka P. Correlation among road unevenness indicators and vehicle vibration response. J. Transp. Eng. 2013; 139(8): 771–786.
- [31] Kropáč O., Můčka P. Be careful when using the International Roughness Index as an indicator of road unevenness. J. Sound Vib. 2005; 287(4–5): 989–1003.
- [32] Můčka P., Granlund J. Is the road quality still better? J. Transp. Eng. 2012; 138(12): 1520–1529.
- [33] Andrén P. Power spectral density approximations of longitudinal road profiles. Int. J. Veh. Des. 2006; 40(1/2/3): 2–14.
- [34] ISO 8608, Mechanical vibration – road surface profiles – reporting of measured data, International Standardization Organization, Geneva, 1995.
- [35] Kollmer H., Kucukay F., Potter K. Measurement and fatigue damage evaluation of road profiles in customer operation. Int. J. Veh. Des. 2011; 56 (1/2/3/4): 106–124.
- [36] Kropáč O., Můčka, P. Indicators of longitudinal unevenness of roads in the USA. Int. J. Veh. Des. 2008; 46(4): 393–415.
- [37] Můčka P. Road waviness and the dynamic tyre force. Int. J. Veh. Des. 2004; 36(2/3): 216–232.
- [38] Kropáč O., Můčka P. Effect of obstacles on roads with different waviness values on the vehicle response. Veh. Syst. Dyn. 2008; 46(3): 155–178.
- [39] Kropáč O., Můčka P. Effects of longitudinal road waviness on vehicle vibration response. Veh. Syst. Dyn. 2009; 47(2): 135–153.
- [40] Gagnon, L. Développement d'un modèle dynamique et quantification de l'influence du profil de la route sur un véhicule. [Ph.D. Thesis]. Laval University, Québec, Canada, 2013.
- [41] Gagnon L., Richard M.J., Masarati P., Morandini M., Doré G. An implicit ring tire model for multibody simulation with energy dissipation. Tire Science and Technology 2014; 42(2): 62–84.
- [42] Gagnon L., Doré G., Richard M.J. An overview of various new road profile quality evaluation criteria: part 1. Int. J. Pav. Eng. 2014; 16(3): 224–238.

## TABLES

Table 1. Percentage difference  $\Delta$  (Eq. (1)) in vibration response for road profile #040214K1.

| $v$<br>[km/h] | Tyre-road contact model                         | $a_{wds}$ | $a_{wps}$ | $F_{dF}$ | $F_{dR}$ | $a_{cb}$ |
|---------------|---|-----------|-----------|----------|----------|----------|
| 60            | Moving averaged profile/tyre-road point contact | -1.1      | -1.6      | -22.5    | -27.1    | -5.6     |
|               | Tyre-enveloping model/tyre-road point contact   | -1.1      | -0.8      | -13.7    | -15.7    | -2.4     |
|               | Tyre-enveloping model/moving averaged profile   | 0         | 0.8       | 11.3     | 15.7     | 3.4      |
| 90            | Moving averaged profile/tyre-road point contact | -1        | -0.8      | -13.1    | -15.7    | -2.2     |
|               | Tyre-enveloping model/tyre-road point contact   | -1        | -0.8      | -8.1     | -9       | -1.1     |
|               | Tyre-enveloping model/moving averaged profile   | 0         | 0         | 5.9      | 7.9      | 1.1      |
| 120           | Moving averaged profile/tyre-road point contact | -0.9      | -0.7      | -8.7     | -10.4    | -1       |
|               | Tyre-enveloping model/tyre-road point contact   | 0         | 0         | -5.8     | -6       | -0.5     |
|               | Tyre-enveloping model/moving averaged profile   | 0.9       | 0.7       | 3.2      | 4.9      | 0.5      |

Table 2. Mean percentage difference  $\Delta$  (Eq. (1)) as a function of velocity for 1600 road profiles

| $v$<br>[km/h] | Tyre-road contact model                         | $a_{wds}$ | $a_{wps}$ | $F_{dF}$ | $F_{dR}$ | $a_{cb}$ |
|---------------|---|-----------|-----------|----------|----------|----------|
| 60            | Moving averaged profile/tyre-road point contact | -2.2      | -2.2      | -18.6    | -21.4    | -5.9     |
|               | Tyre-enveloping model/tyre-road point contact   | -0.9      | -0.9      | -10      | -10.9    | -2.4     |
|               | Tyre-enveloping model/moving averaged profile   | 1.3       | 1.3       | 10.6     | 13.5     | 3.7      |
| 90            | Moving averaged profile/tyre-road point contact | -1.1      | -1.1      | -11.9    | -13.5    | -2.7     |
|               | Tyre-enveloping model/tyre-road point contact   | -0.5      | -0.5      | -6.7     | -7.2     | -1.1     |
|               | Tyre-enveloping model/moving averaged profile   | 0.6       | 0.6       | 6.0      | 7.4      | 1.6      |
| 120           | Moving averaged profile/tyre-road point contact | -0.5      | -0.6      | -8.3     | -9.6     | -1.6     |
|               | Tyre-enveloping model/tyre-road point contact   | -0.2      | -0.3      | -4.8     | -5.2     | -0.6     |
|               | Tyre-enveloping model/moving averaged profile   | 0.2       | 0.3       | 3.8      | 4.9      | 1.0      |

Table 3. Mean percentage difference  $\Delta$  (Eq. (1)) as a function of the road surface type for  $v = 90$  km/h

| Road surface type                                    | IRI [mm/m]       | Tyre-road contact model                         | $a_{wds}$ | $a_{wps}$ | $F_{dF}$ | $F_{dR}$ | $a_{cb}$ |
|--|------------------|---|-----------|-----------|----------|----------|----------|
| SPS-2<br>Doweled jointed plain<br>concrete pavements | $1.41 \pm 0.393$ | Moving averaged profile/tyre-road point contact | -1.4      | -1.4      | -11.4    | -13.3    | -3.2     |
|  |                  | Tyre-enveloping model/tyre-road point contact   | -0.1      | -0.3      | -4.7     | -5.1     | 0        |
|  |                  | Tyre-enveloping model/moving averaged profile   | 1.4       | 1.1       | 7.3      | 9.1      | 3.3      |
| SPS-4<br>Rigid pavements                             | $1.38 \pm 0.645$ | Moving averaged profile/tyre-road point contact | -0.9      | -1        | -10.7    | -12.2    | -2.5     |
|  |                  | Tyre-enveloping model/tyre-road point contact   | 2.4       | 2.5       | -2.7     | -3       | 2        |
|  |                  | Tyre-enveloping model/moving averaged profile   | 3.4       | 3.5       | 9.1      | 10.5     | 4.6      |
| SPS-5<br>Asphalt concrete<br>pavements               | $1.45 \pm 0.702$ | Moving averaged profile/tyre-road point contact | -0.9      | -1        | -12.9    | -14.6    | -2.4     |
|  |                  | Tyre-enveloping model/tyre-road point contact   | -0.4      | -0.5      | -6.8     | -7.3     | -1       |
|  |                  | Tyre-enveloping model/moving averaged profile   | 0.5       | 0.6       | 7.2      | 8.7      | 1.4      |
| SPS-6<br>Rehabilitated jointed<br>PCC pavements      | $1.71 \pm 0.897$ | Moving averaged profile/tyre-road point contact | -1        | -1.1      | -12.7    | -14.1    | -2.6     |
|  |                  | Tyre-enveloping model/tyre-road point contact   | -0.7      | -0.6      | -8       | -8.1     | -1.5     |
|  |                  | Tyre-enveloping model/moving averaged profile   | 0.3       | 0.4       | 5.4      | 7        | 1.2      |

Table 4. Measured and simulated frequency-weighted seat vertical RMS acceleration for road section “Essais AM” and  $v = 67$  km/h as a function of distance.

| $l$ [m]   | 0–100 | 100–200 | 200–300 | 300–400 | 400–500 | 500–600 |
|---|-------|---------|---------|---------|---------|---------|
| $a_{ws}$ [ $m/s^2$ ] – measured                                     | 0.683 | 0.946   | 0.818   | 0.855   | 0.656   | 0.669   |
| $a_{ws}$ [ $m/s^2$ ] – measured (0.2–10 Hz)                         | 0.527 | 0.744   | 0.644   | 0.579   | 0.496   | 0.512   |
| $a_{ws}$ [ $m/s^2$ ] – simulated –<br>tyre-road point contact model | 0.410 | 0.466   | 0.498   | 0.323   | 0.555   | 0.317   |
| $a_{ws}$ [ $m/s^2$ ] – simulated –<br>moving averaged profile       | 0.409 | 0.462   | 0.498   | 0.322   | 0.553   | 0.316   |
| $a_{ws}$ [ $m/s^2$ ] – simulated –<br>rigid ring tyre model         | 0.357 | 0.523   | 0.542   | 0.374   | 0.368   | 0.422   |
| $IRI_L$ [mm/m] – left track   | 4.22  | 5.65    | 5.45    | 5.68    | 4.92    | 5.00    |
| $IRI_R$ [mm/m] – right track  | 4.70  | 7.98    | 6.39    | 5.77    | 7.44    | 6.57    |
| $IRI_{LR}$ [mm/m] – left and right track                            | 4.46  | 6.81    | 5.92    | 5.72    | 6.18    | 5.78    |
| $C_L$ [ $10^{-6}$ rad m] – left track                               | 6.16  | 6.31    | 8.65    | 8.76    | 6.55    | 7.51    |
| $C_R$ [ $10^{-6}$ rad m] – right track                              | 5.36  | 11.78   | 12.29   | 7.46    | 9.60    | 8.27    |
| $C_{LR}$ [ $10^{-6}$ rad m] – left and right track                  | 5.75  | 8.62    | 10.31   | 8.08    | 7.93    | 7.88    |
| $w_L$ – left track  | 2.61  | 2.33    | 2.54    | 2.29    | 2.45    | 2.50    |
| $w_R$ – right track   | 2.49  | 2.70    | 2.76    | 2.37    | 2.45    | 2.52    |
| $w_{LR}$ – left and right track                                     | 2.55  | 2.52    | 2.65    | 2.33    | 2.45    | 2.51    |

## FIGURES

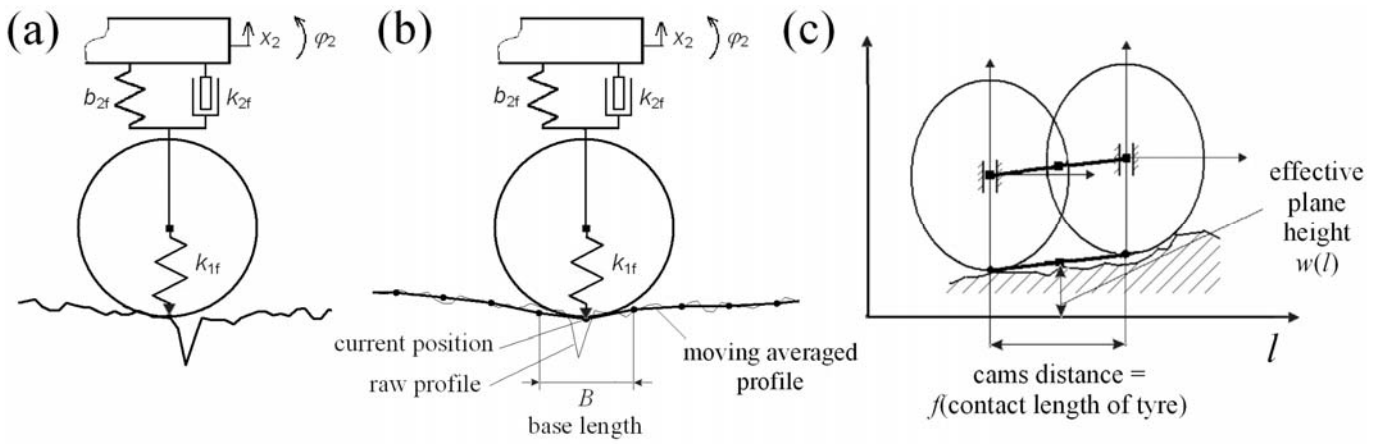


Figure 1. Scheme of the three tyre-road contact models: (a) the tyre-road point contact model; (b) the moving averaged road profile; (c) the tyre-enveloping model.

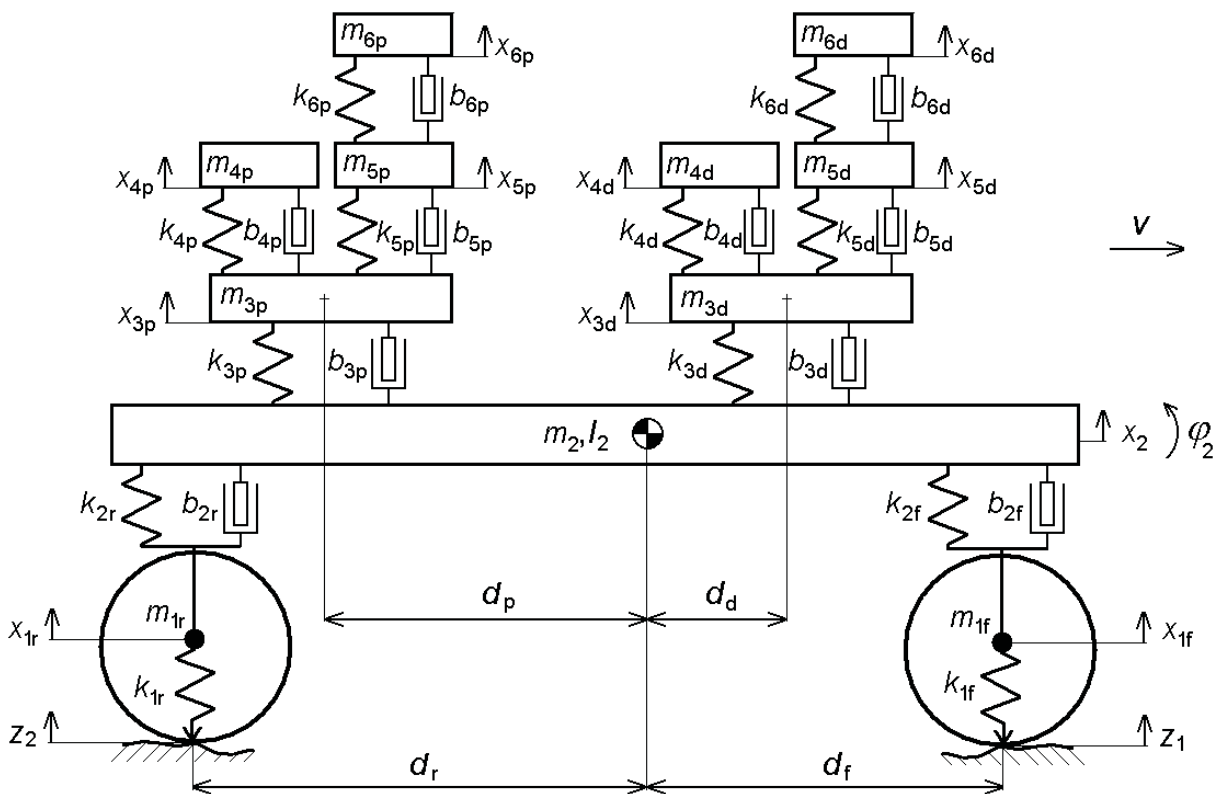


Figure 2. Longitudinal planar model of an automobile with 12-DOF.

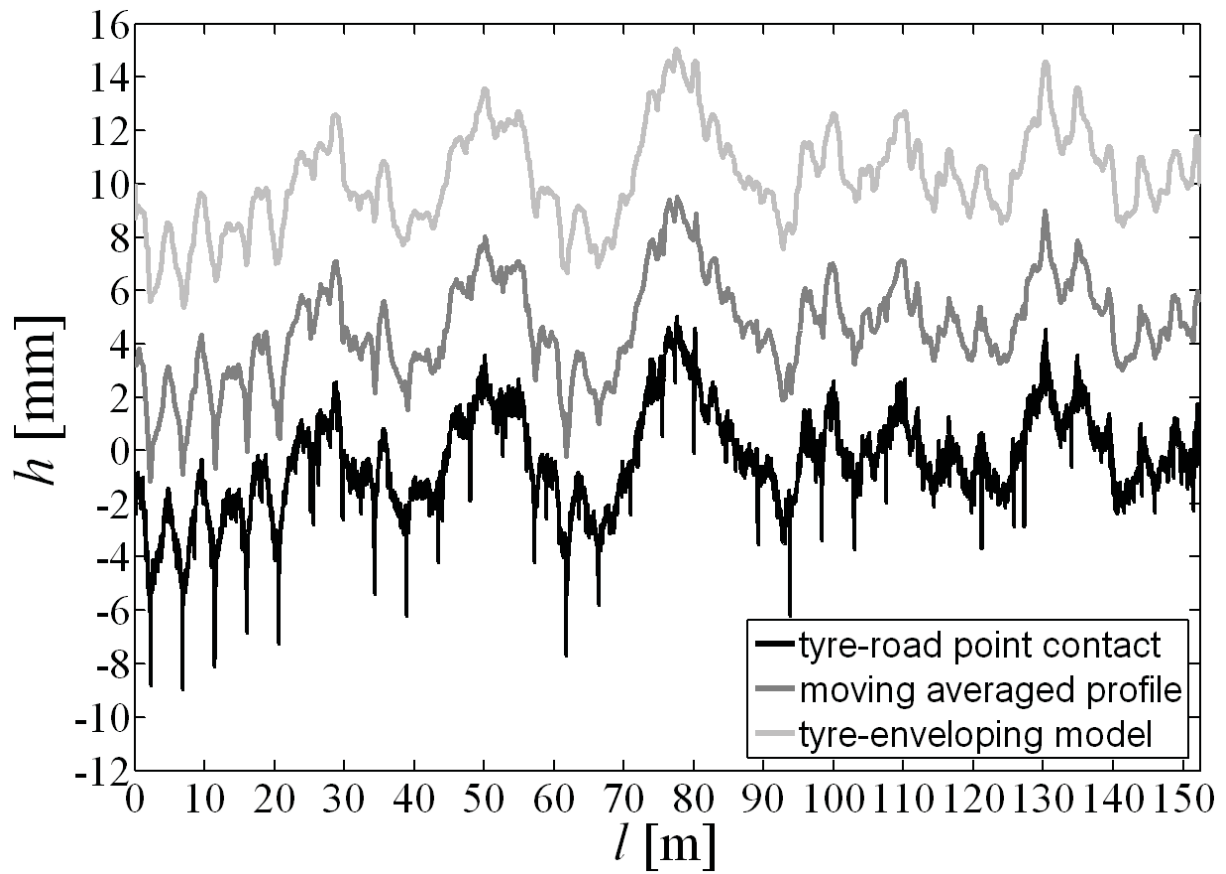


Figure 3. Road elevation of the right track of the road profile #040214K1 (profiles are shifted vertically by 5 mm).

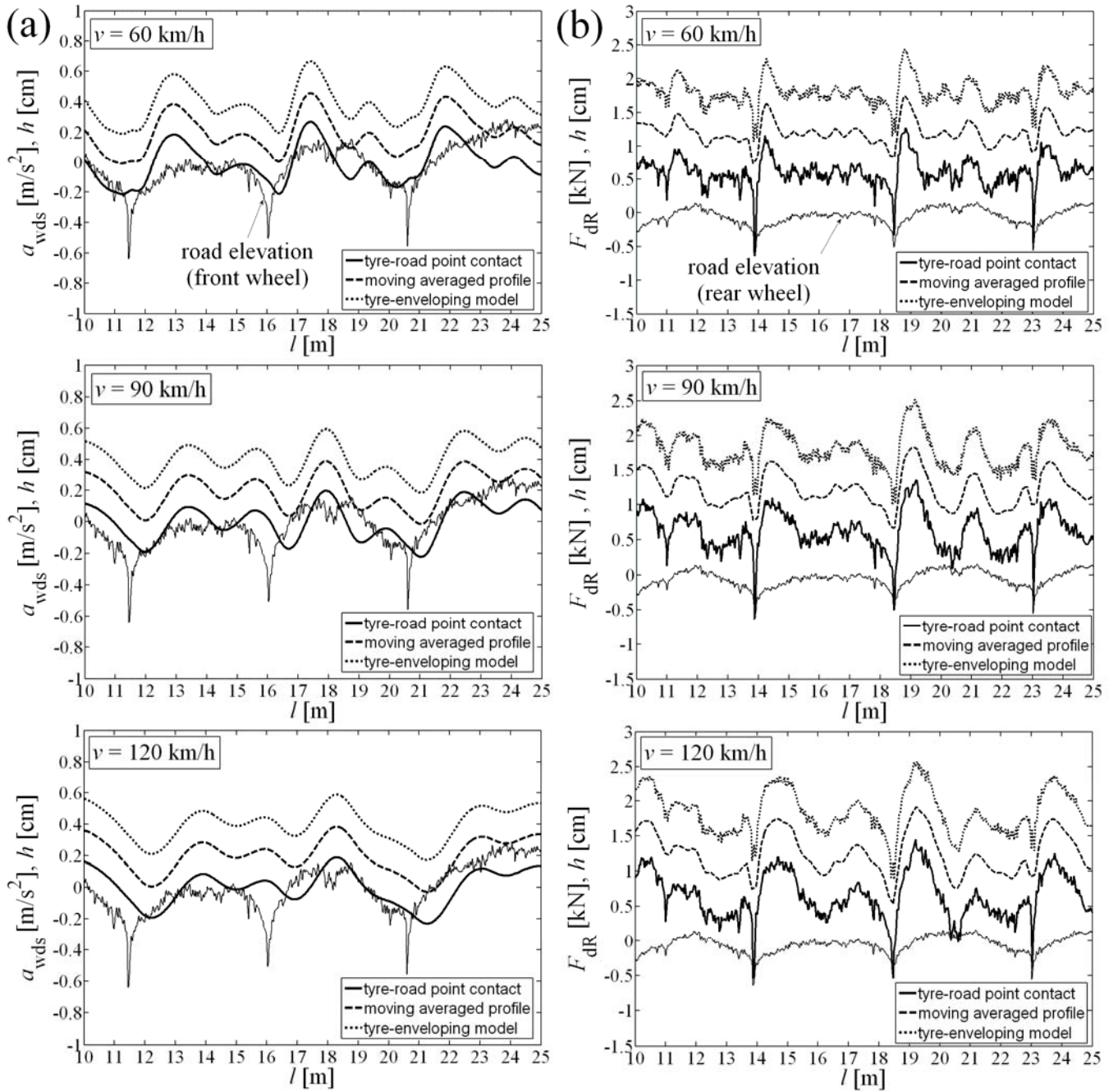


Figure 4. (a) Frequency-weighted acceleration  $a_{wds}$  (shifted vertically by  $0.2 \text{ m/s}^2$ ) and (b) rear axle dynamic tyre force  $F_{dR}$  (shifted vertically by  $0.6 \text{ kN}$ ) as a function of velocity and tyre-road contact models (road section #040214K1).

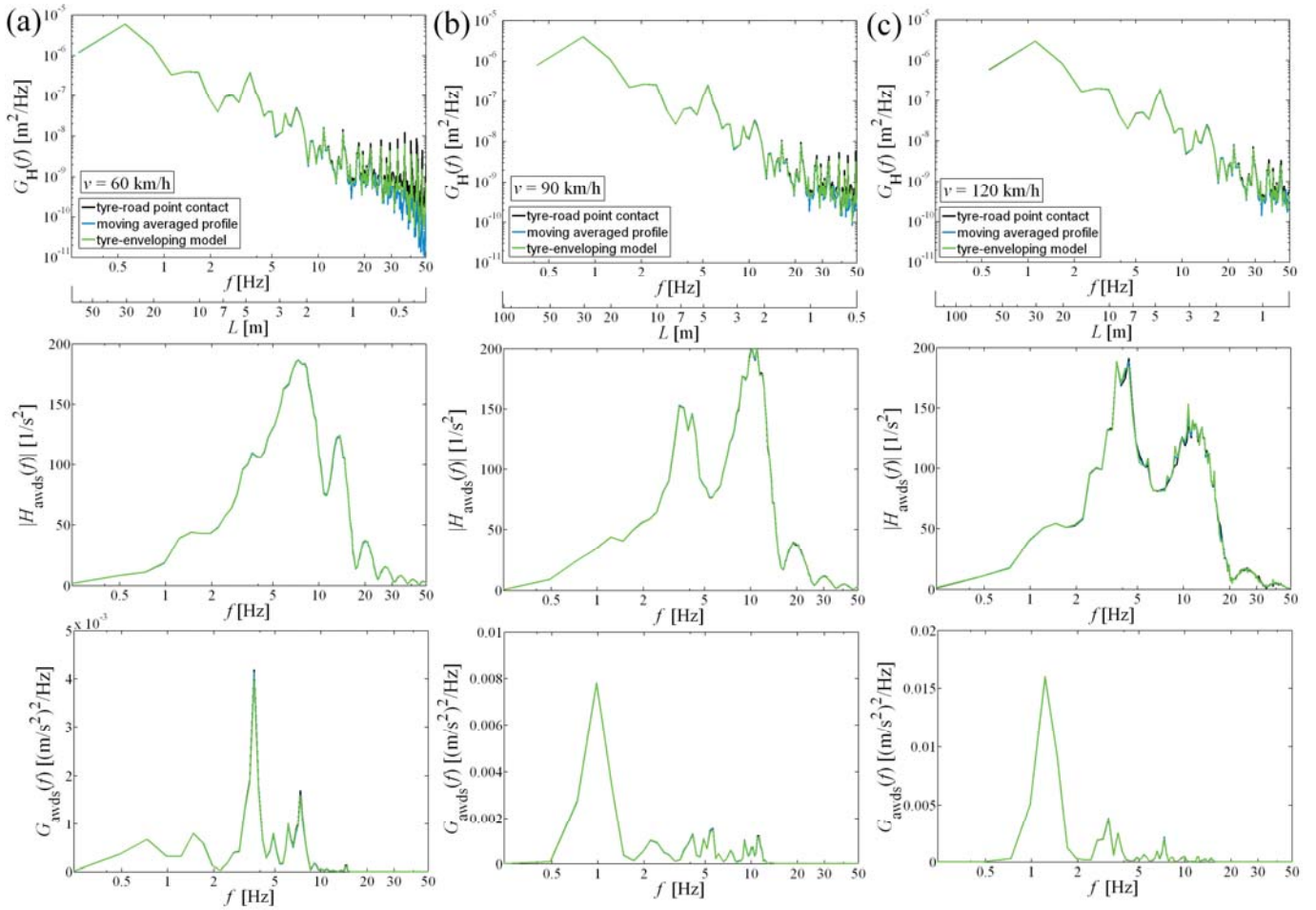


Figure 5. Road elevation spectrum,  $G_H(f)$ , estimated transfer function,  $H_{awds}(f)$ , and frequency-weighted acceleration on driver's seat spectrum,  $G_{awds}(f)$ , for velocities: (a) 60 km/h; (b) 90 km/h; (c) 120 km/h.

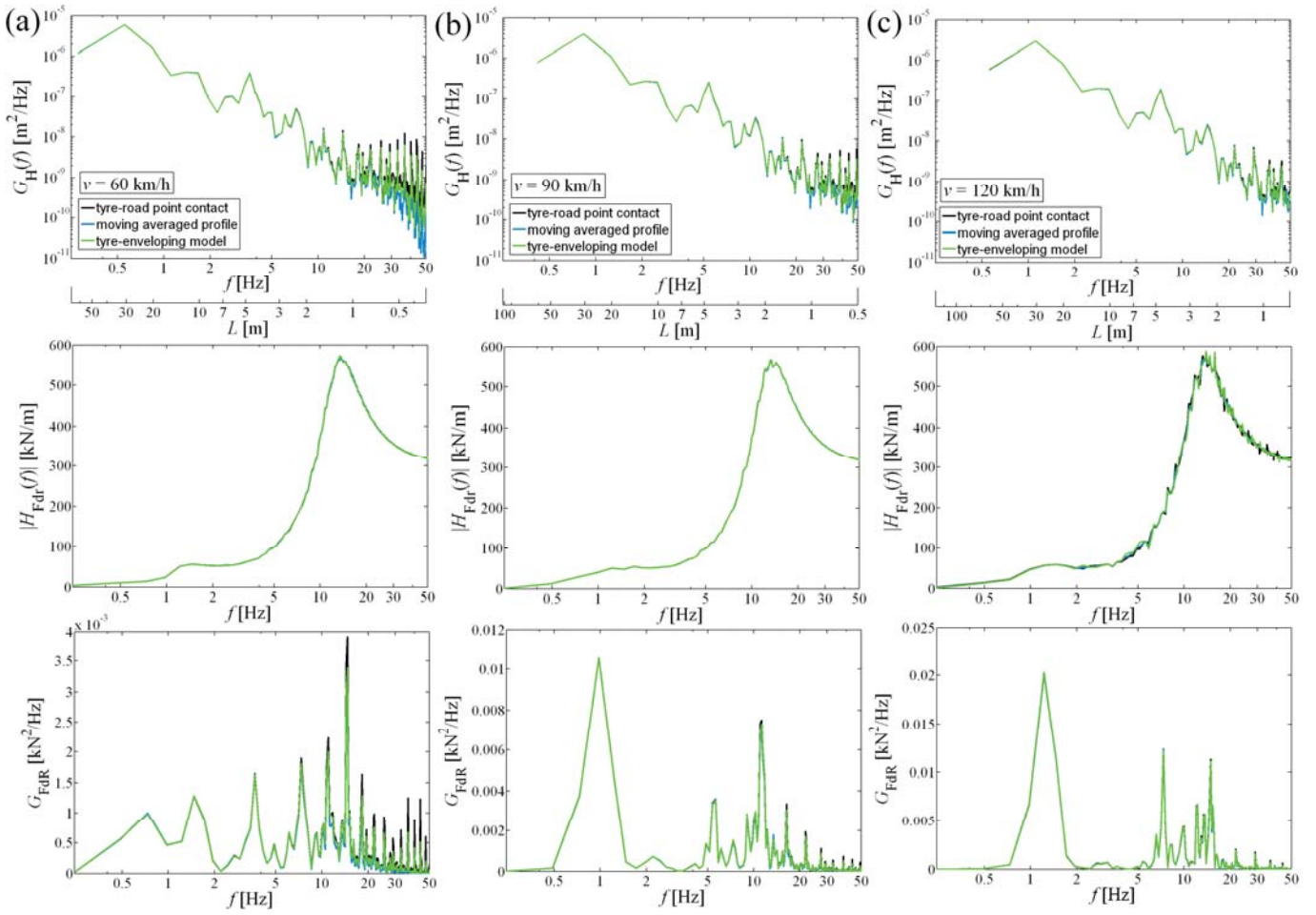


Figure 6. Road elevation spectrum,  $G_H(f)$ , estimated transfer function,  $H_{awds}(f)$ , and rear-axle dynamic tyre force,  $G_{FDR}(f)$ , for velocities: (a) 60 km/h; (b) 90 km/h; (c) 120 km/h.

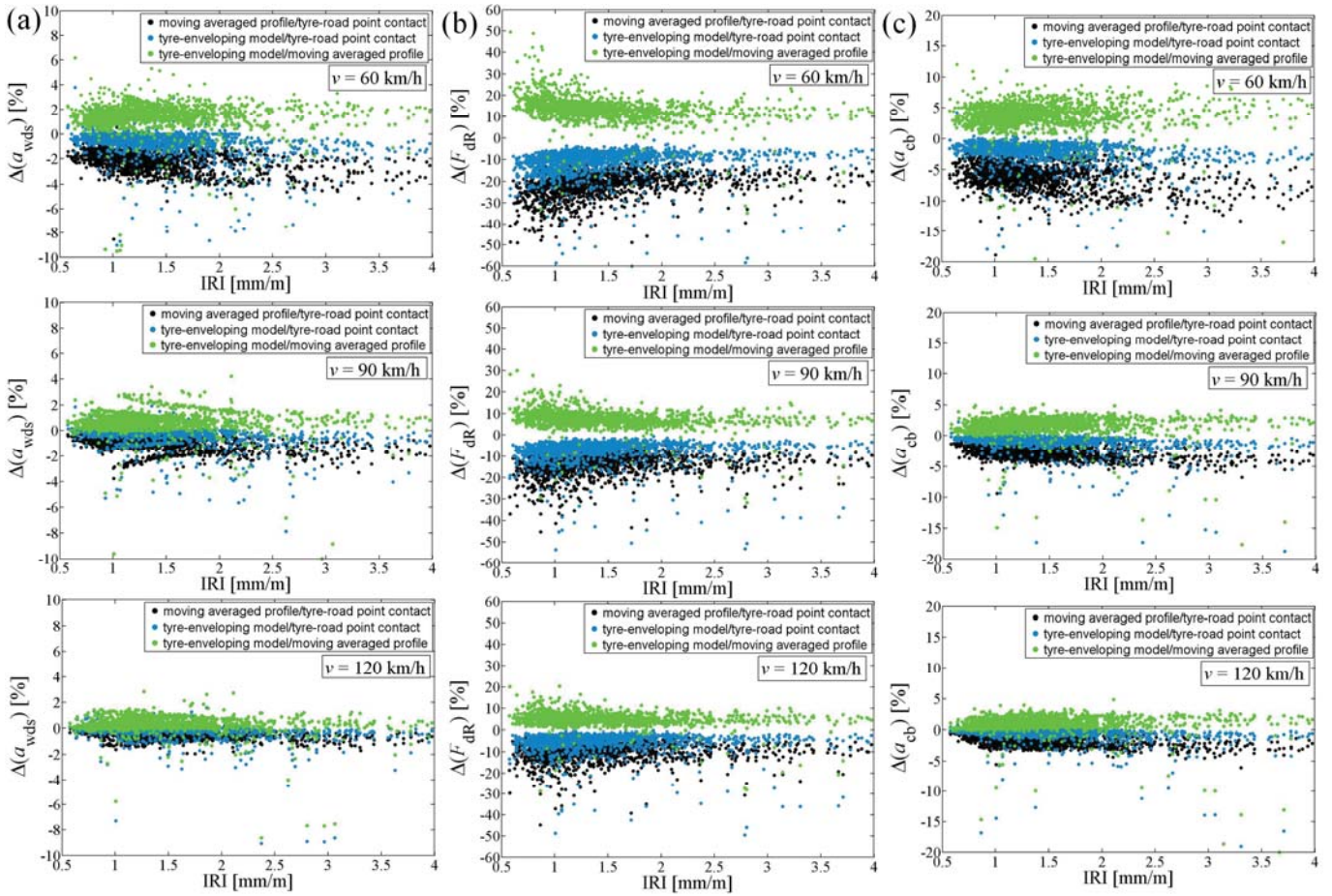


Figure 7. Percentage difference in vibration response for 1600 road profiles as a function of road roughness and velocity: (a) frequency-weighted acceleration on the driver's seat,  $a_{\text{wds}}$ ; (b) dynamic tyre force,  $F_{\text{dR}}$ , and (c) car body vertical acceleration,  $a_{\text{cb}}$ .

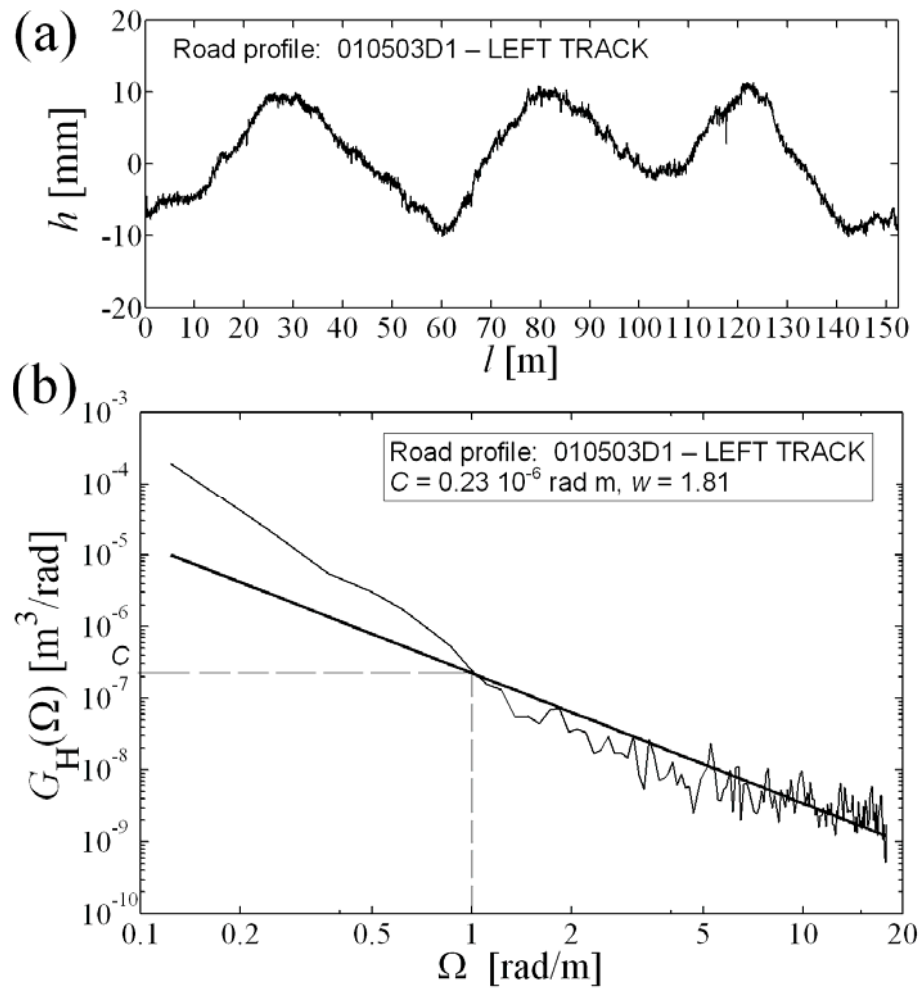


Figure 8. (a) Road elevation and (b) Road elevation power spectral density (road section #010503D1).

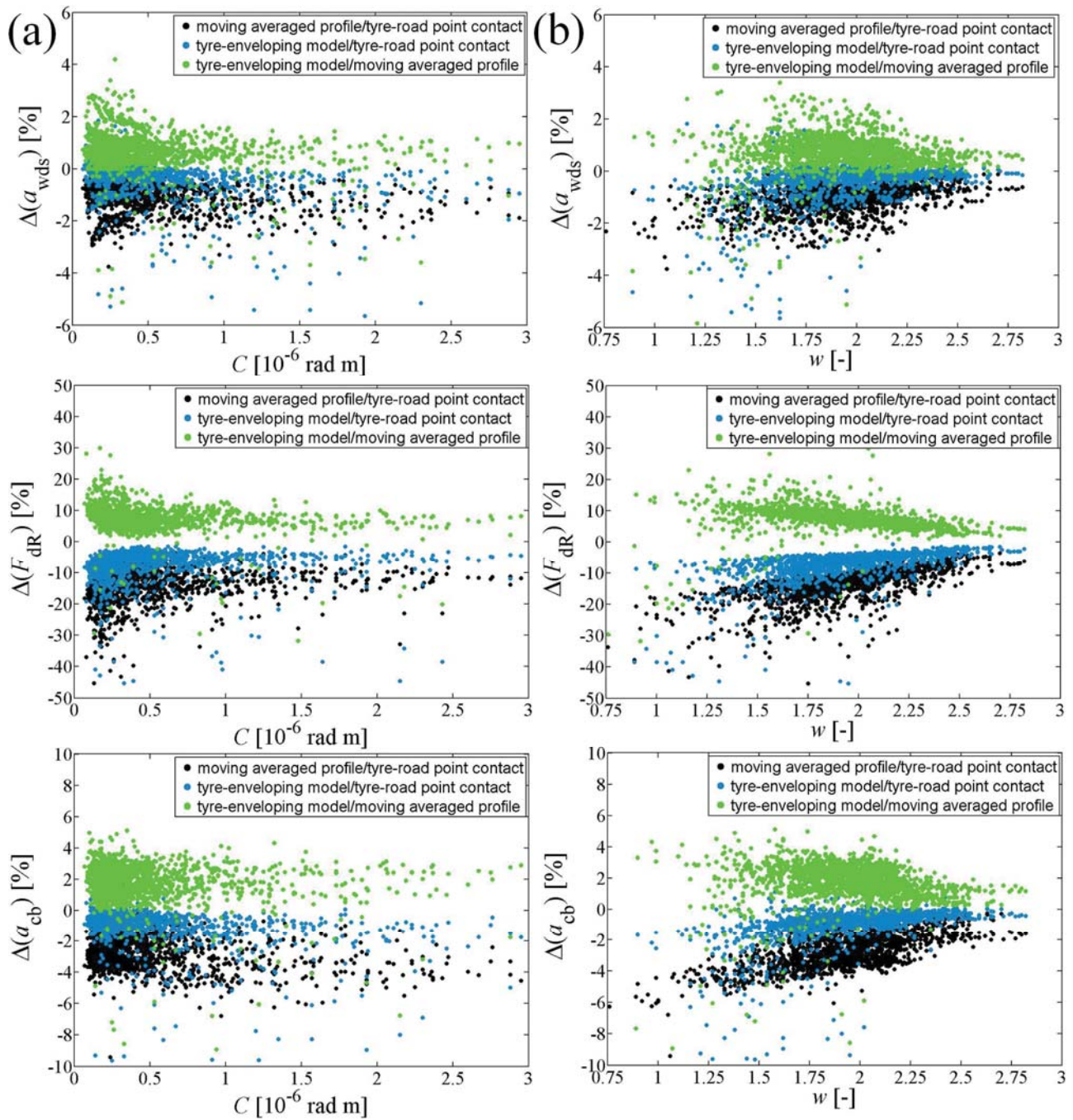


Figure 9. Percentage difference in vibration response for 1600 road profiles and  $v = 90$  km/h as a function of (a) unevenness index,  $C$ , (b) road waviness,  $w$  ( $a_{wds}$  – first row;  $F_{dR}$  – second row;  $a_{cb}$  – third row).

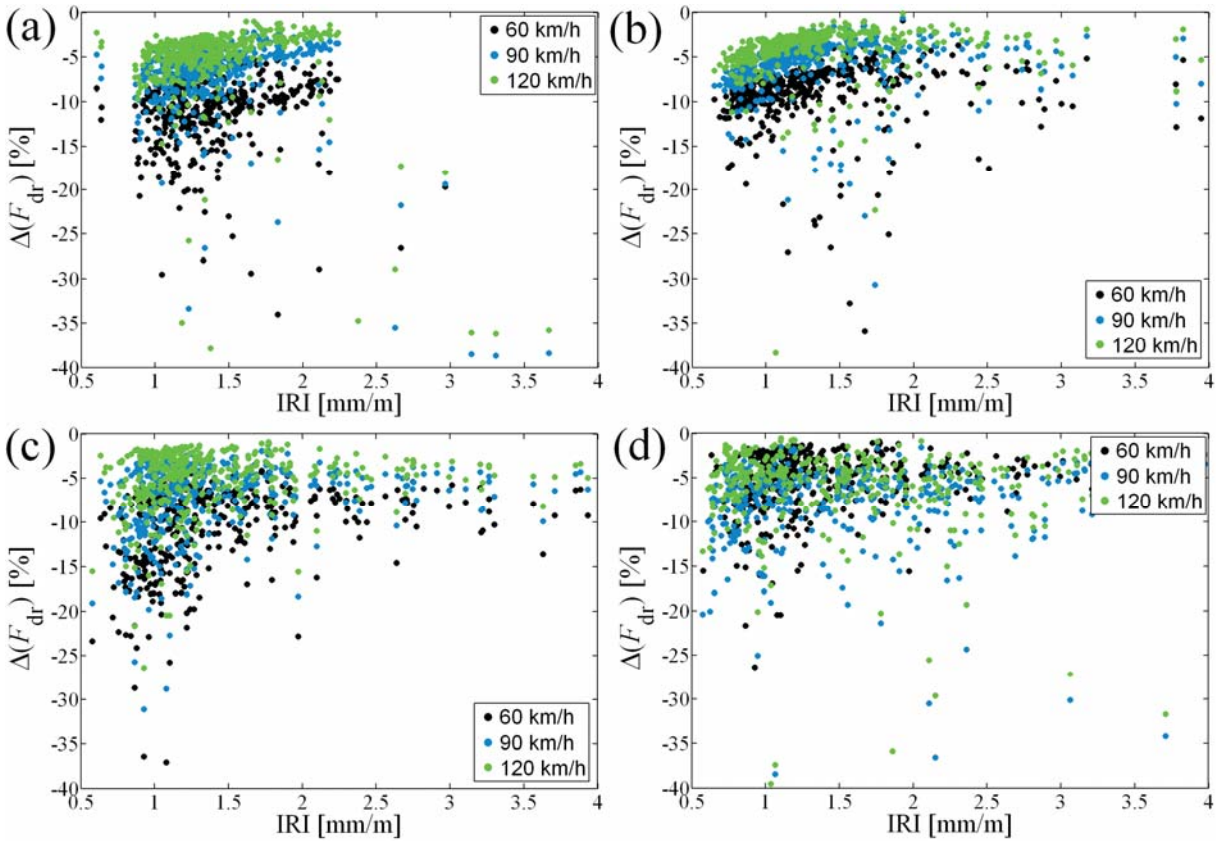


Figure 10. Percentage difference in vibration response for the tyre-enveloping model and the tyre-road point contact model for rear-axle dynamic tyre force,  $F_{dr}$ , as a function of the road surface type: (a) SPS-2; (b) SPS-4; (c) SPS-5; (d) SPS-6.

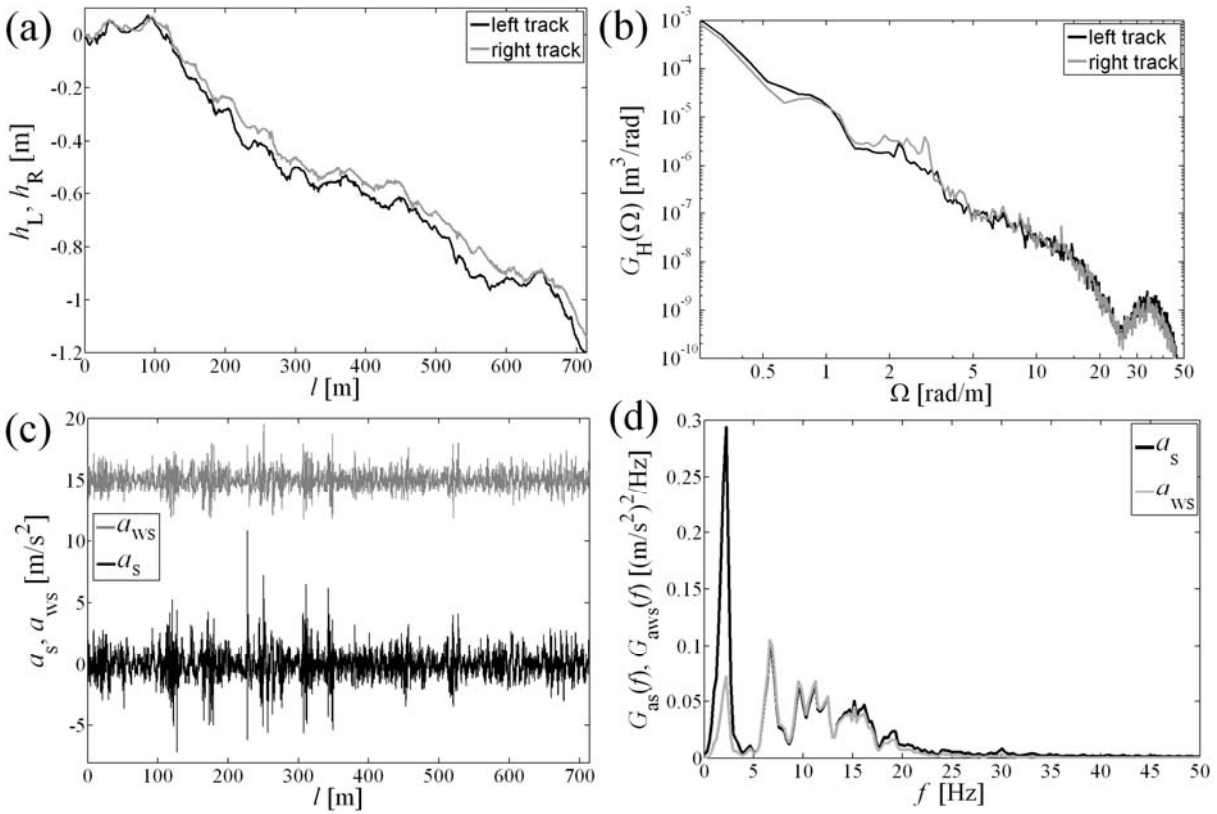


Figure 11. (a) Road elevation; (b) Road elevation PSD; (c) Measured seat vertical acceleration,  $a_s$ , and frequency-weighted acceleration,  $a_{ws}$  (shifted vertically by  $15 \text{ m/s}^2$ ) on the semi-trailer truck, and (d) Acceleration PSD (Road section “Essais AM”).

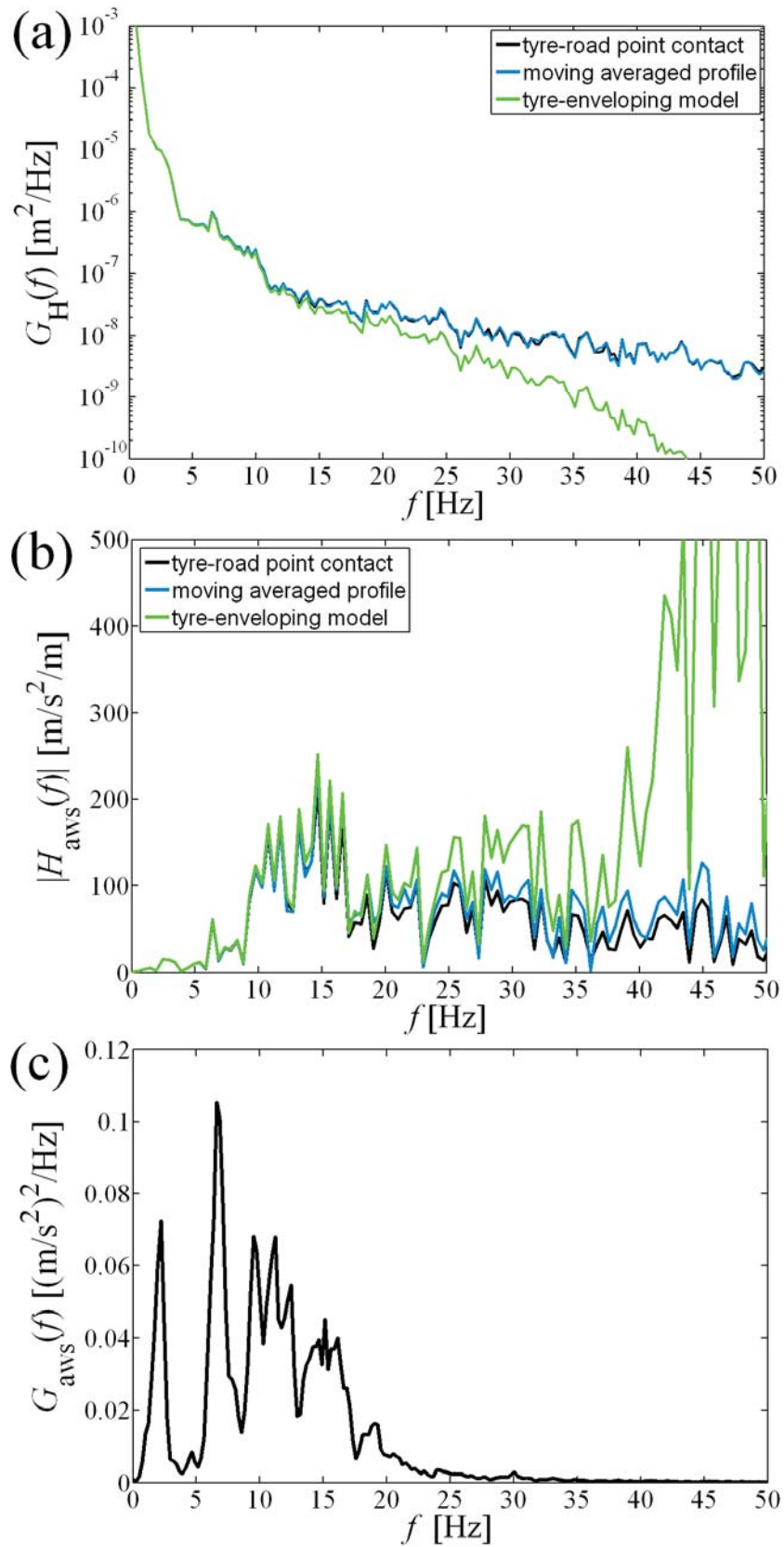


Figure 12. (a) Road elevation spectrum,  $G_H(f)$ , (b) estimated transfer function,  $H_{\text{aws}}(f)$ , and (c) measured frequency-weighted seat vertical acceleration spectrum,  $G_{\text{aws}}(f)$ , for  $v = 67$  km/h and road section “Essais AM”.

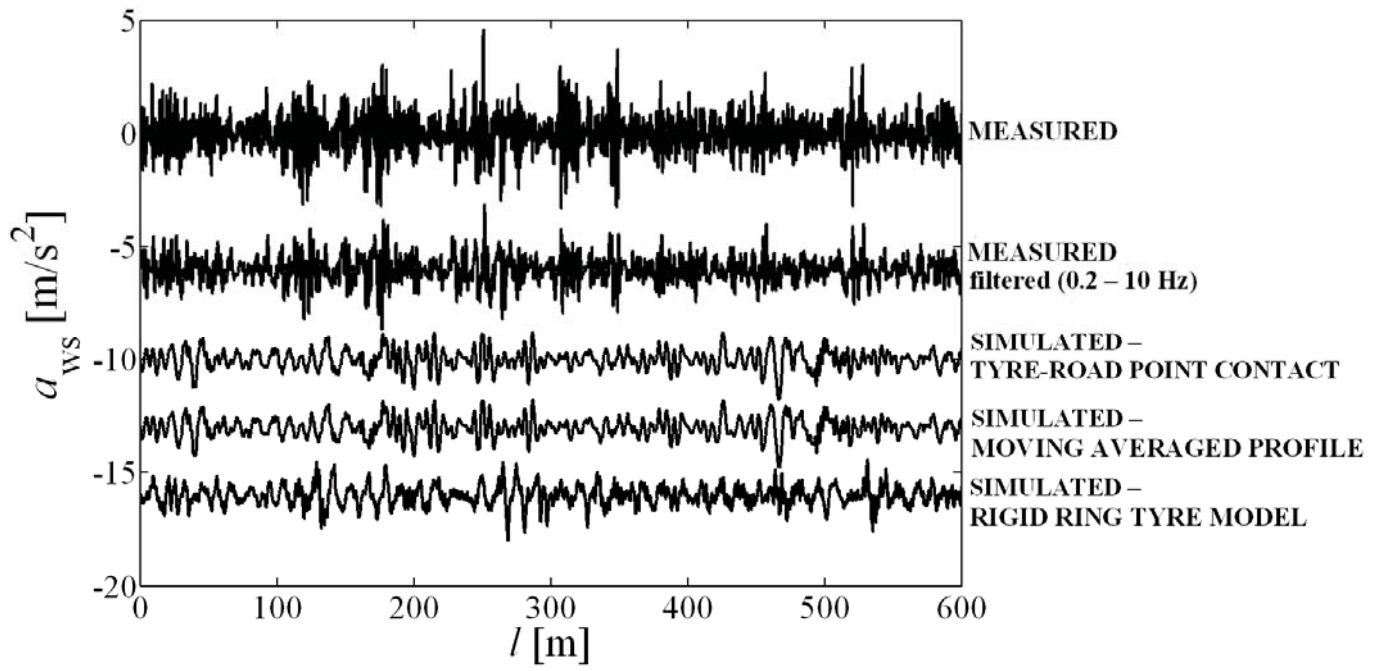


Figure 13. Measured and simulated frequency-weighted acceleration  $a_{ws}$  for three tyre-road contact models and multibody semi-trailer truck ( $v = 67$  km/h).